Hydrol. Earth Syst. Sci. Discuss., https://doi.org/10.5194/hess-2018-254
Manuscript under review for journal Hydrol. Earth Syst. Sci.
Discussion started: 14 May 2018


Hydrology and Earth System Sciences
Discussions
Open Access

# Factors influencing spring and summer areal snow ablation and snowcover depletion in alpine terrain: detailed measurements from the Canadian Rockies

**Michael Schirmer[1,2] and John W. Pomeroy[1]**

[1] Centre for Hydrology, University of Saskatchewan, Canada

[2] WSL Institute for Snow and Avalanche Research SLF, Davos, Switzerland

Correspondence to: Michael Schirmer (michael.schirmer@slf.ch)

**Abstract**

The spatial distribution of snow water equivalent (SWE) and melt are important to estimating areal melt rates and snowcover depletion dynamics but are rarely measured in detail during the late ablation period. This study contributes the result of high resolution observations made using large numbers of sequential aerial photographs taken from an Unmanned Aerial Vehicle on an alpine ridge in the Fortress Mountain Snow Laboratory in the Canadian Rocky Mountains from May to July. With Structure-from-Motion and thresholding techniques, spatial maps of snow depth, snowcover and differences in snow depth during ablation were generated in very high resolution as proxies for spatial SWE, spatial ablation rates, and snowcover depletion (SCD). The results indicate that the initial distribution of SWE was highly variable due to overwinter snow redistribution and the subsequent distribution of ablation rates was also variable due to albedo, slope/aspect and other unaccountable differences. However, the initial distribution of SWE was five times more variable than that of subsequent ablation rates, even though ablation differences were substantial, with variability by a factor of two between north and south aspects, and somewhat persistent over time. Ablation rate patterns had an insubstantial impact on SCD curves, which were overwhelmingly governed by the initial distribution of SWE. The reasons for this are that variations in irradiance to slopes on north and south aspects in the near-summer solstice period are relatively small and only a weak spatial correlation developed between initial SWE and ablation rates. Previous research has shown that spatial correlations between SWE and

Hydrol. Earth Syst. Sci. Discuss., https://doi.org/10.5194/hess-2018-254
Manuscript under review for journal Hydrol. Earth Syst. Sci.
Discussion started: 14 May 2018




ablation rates can strongly influence SCD curves. The results presented here are in contrast to alpine, shrub tundra and forest observations taken during ablation at higher latitudes and/or earlier in spring but in agreement with other near-summer observations in alpine environments. Whilst variations in net solar irradiance to snow were due to small scale variations in localized dust deposition from eroded ridgetop soil and larger scale differences in slope and aspect, variations in SWE were due to intense over-winter blowing snow storms with deposition from multiple directions of snow transport to incised gullies and slope breaks. This condition differs considerably from situations where wind transport from primarily one direction leads to preferential SWE loading on slopes of particular aspects, which can lead to a spatial correlation between SWE and ablation rate. These findings suggest that in near-summer solstice conditions and environments where snow redistribution is substantial, then mountain SCD curves can be calculated using the spatial distribution of SWE alone, and that hydrological and atmospheric models need to implement a realistic distribution of SWE in order to do this.

## 1 Introduction

The spatial variability of snow water equivalent (SWE) during melt exerts an important control on catchment or grid scale meltwater generation (Pomeroy et al., 1998). Terrain-induced differences in precipitation and terrain and vegetation-induced differences in snow redistribution lead to a spatially variable distribution of SWE at the start of the melting season. In many environments, the temporal progression of snow-cover depletion (SCD) has been found to be governed primarily by the premelt distribution of SWE (Shook and Gray, 1996; Donald et al., 1995; Marsh and Pomeroy, 1996; Luce et al., 1998, 1999; Pomeroy et al. 1998; Pomeroy et al. 2001; Egli et al., 2012). All of these studies have explained the observations by suggesting that the main deposition patterns remained during melt and that the statistical properties of SWE distribution control SCD. This is parameterised as the SCD curve in many hydrological and land surface models (Kuchment and Gelfan, 1996; Verseghy, 2000; Essery and Pomeroy, 2004) where a spatially uniform ablation rate is applied to a frequency distribution of SWE to calculate areal ablation rates and SCD during melt.

However, spatially varying melt rates – caused by differences in insolation due to aspect (Marks and Dozier, 1992), net solar irradiance due to albedo differences (Skiles et al., 2015), internal energy storage due to deep, cold snow (DeBeer and Pomeroy, 2010), turbulent

Hydrol. Earth Syst. Sci. Discuss., https://doi.org/10.5194/hess-2018-254
Manuscript under review for journal Hydrol. Earth Syst. Sci.
Discussion started: 14 May 2018


Hydrology and Earth System Sciences
Open Access
Discussions

transfer (Pohl et al., 2006) and advected energy due to bare ground or exposed vegetation (Mott et al., 2011; 2013; Ménard et al., 2014) can alter this pre-melt SWE distribution and, when correlated to SWE, result in a spatial variability to SCD (Faria et al., 2000; Pomeroy et al., 2001; Essery and Pomeroy, 2004; Dornes et al., 2008a, b; DeBeer and Pomeroy, 2010). For instance in the boreal forest, snow interception by needleleaf trees reduces SWE accumulation, but higher ablation rates near tree trunks accelerate melt – this induces a negative spatial covariance between premelt SWE and melt rates that causes a strong bias in SCD (Faria et al., 2000). Pomeroy et al. (2003) took measurements of energy fluxes to snowpacks using eddy correlation and slope based radiometers and snow ablation using spatially distributed snow surveys in a Yukon mountain valley in April and found that whilst ablation was proceeding rapidly on south facing slopes where snow was initially shallow, snow accumulation was still occurring on north facing slopes where a large drift had formed. The different snow surface states and impact of prevailing winds and slope and aspect resulted in energy fluxes melting snow on south facing slopes and cooling snow on north facing slopes. As a consequence, a common SCD was not viable over the whole valley. In Yukon and the Canadian Rockies, subsequent studies found melt variations to be important in controlling snow ablation and SCD (Pomeroy et al., 2003; 2004; Dornes et al., 2008a, b; DeBeer and Pomeroy, 2009; 2010). Pomeroy et al. (2004) reported that different spatial scales and landscape classes influence melt rates to be positively or negatively correlated to pre-melt SWE throughout melt in a wide variety of cold regions mountain environments. Dornes et al. (2008a, b) found that hydrological models and land surface schemes that did not consider slope and aspect impacts on melt as well as initial SWE could not be calibrated to produce realistic SCD curves or streamflow discharge hydrographs. DeBeer and Pomeroy (2010) found that melt rate variations were quite important in the Canadian Rockies in early melt. In contrast, Grünewald et al. (2010) observed only a weak relationship between topographic and meteorological variables to spatial melt rates in a Swiss mountain valley; the relationship decreased later in the melt season. They found using Terrestrial Laser Scanning (TLS) that the variability of pre-melt SWE was much more variable than spatial melt differences. Winstral and Marks (2002), Magnusson et al. (2011) and Winstral et al. (2013) concluded that spatial melt models which do not include spatial SWE variations caused by wind effects were not sufficient to model runoff in mountains. Anderton et al. (2004) found that pre-melt SWE was more important than spatial melt differences for explaining SCD in the Pyrenees.

Hydrology and Earth System Sciences Discussions

When focusing on studies in alpine terrain without a larger vegetation effect on melt (e.g. DeBeer and Pomeroy, 2010; Egli et al. 2012) it still remains unclear whether spatial variable snowmelt in addition to spatially variable SWE should be considered in calculating SCD. Much of this uncertainty is due to the limited number of detailed measurements available and the uncertainty of distributed model results. There are likely to be fundamental differences in the sequence of ablation between relatively warm and cold mountain environments due to the effect of internal energy deficits in delaying melt of deep snowpacks (DeBeer and Pomeroy, 2010). But there are also substantial differences in solar irradiance as the summer solstice is approached – as shown in Fig. 1 in April at 50$^{o}$ N there is a 17 MJ m$^{-2}$ difference between irradiance on 30% N and S facing slopes, but by solstice this decreases to 2.5 MJ m$^{-2}$. The variation in observations and model results for alpine terrain creates uncertainty in the relative importance of spatial melt rates and SWE to determine SCD and areal ablation rates. To address this uncertainty an extremely high spatial resolution digital surface model dataset was collected over an alpine ridge in the Canadian Rockies using an Unmanned Aerial Vehicle (UAV) and Structure from Motion (SfM) analysis to repeatedly determine snow depth and snow depth differences during a melt season as proxies of initial SWE and sequential, spatial melt rates. Analysis over several spatial scales was conducted to correlate variables that might influence melt to measured spatial melt rates and investigate the influence of initial SWE and spatial variation in melt on SCD and areal mean melt over an alpine ridge in high mountain terrain.

## 2 Data and methods

### 2.1 Site description

The study area is located in the Canadian Rocky Mountains in southern Alberta, Canada. Figure 2a shows a topographic map of the study area, an alpine ridge in a NE – SW orientation. On both sides of the ridge the slope steepens to up to 40 deg. Gullies and small scale aspect variations can be found in the slopes on both sides of the ridge. Extreme south and north aspects are underrepresented in the snow covered area at the beginning of the study period (Fig. 2b). Vegetation played a role in snow deposition patterns, mainly in the lee of shrubs and clusters of small trees in krummholz with heights up to 2 m. Areas within these vegetation clusters were excluded from the study as vegetation degraded the digital surface models (DSMs) derived from UAV SfM photogrammetry (see section 2.4).

Two weather stations are located at the ridge, one on top of the ridge (Fortress Ridge - FRG) and one in a south facing slope (Fortress Ridge South - FRS, Fig. 2a). The local Fortress Mountain Snow Laboratory within the regional Canadian Rockies Hydrological Observatory provided five more weather stations within less than 2 km distance of the ridge, which were used to interpret weather situations and for quality control.

## 2.2 UAV Data acquisition

A "Sensefly Ebee RTK" fixed wing UAV was used with a modified consumer-grade Canon Elph compact RGB camera. As a base station a Leica GS15 differential GPS system was used, which communicated with the UAV to tag captured images with corrected geolocations. Additionally, ground control points were measured with this differential GPS system, which improved the quality of the Digital Surface Models (DSMs) generated. For a more detailed description of the UAV and the usage please refer to Harder et al. (2016). An area of 666 x 470 m was separated into two subareas because of battery restrictions on flight areas (Fig. 2a, red polygons). Each flight lasted approximately 20 min. The flight altitude was chosen to be 100 m over the ridge top, which resulted in an approximate resolution (ground sampling distance) of smaller than 4 cm. A lateral overlap of the images of 85% and a longitudinal overlap of 75% was chosen as suggested by the manufacturer for difficult terrain. Ideally, four flights in total were made each sampling day, two for each subarea with perpendicular flight plans. Weather conditions and technical problems often allowed only a part of this program. Wind speeds over 14 m/s or occurrence of precipitation restricted flying, while camera malfunctions or connection issues with the Leica GPS base station were the most typical technical limitations.

## 2.3 Accuracy evaluation and manual measurements

The accuracy assessment of this rather new method to determine snow depth was given a high priority and is described in detail by Harder et al. (2016) for this environment and others. In short, 100 differential GPS measurements on bare ground were taken. Approximately 60% of the area was bare at the beginning of the study period which allowed distribution of GPS ground measurements over a large part of the study area (Fig. 3a) and

Hydrol. Earth Syst. Sci. Discuss., https://doi.org/10.5194/hess-2018-254
Manuscript under review for journal Hydrol. Earth Syst. Sci.
Discussion started: 14 May 2018


thus widespread detection of any general misalignment of DSMs or local tilts. These points could be used for all available flights. Differential GPS measurements were also taken at the snow surface on the day of the specific flights, but technical problems often allowed only limited additional time for these surveys. For most of the days up to 20 differential GPS measurements on snow could be taken. At these GPS measurement points, snow depth was also manually measured and snow density was measured at approximately each third of these points. Density measurements were not sufficient to confidently estimate SWE from snow depth into SWE and ablation rates from differences in snow depth. As such the originally measured quantities are analysed and interpreted as proxies for ablation and SWE in the text.

Harder et al. (2016) described errors and accuracies of the UAV measurements in detail. In short, from 100 measurements on bare ground, the root mean square errors of bare ground surface elevation ranged between 4 and 15 cm with a mean of less than 9 cm. Over snow with fewer measurements an increase in these error measures could not be detected. A signal-to-noise ratio (SNR) was used to ensure that the signal of the UAV was sufficiently larger than the error, defined as mean of the signal divided by the standard deviation of the error . The potential impact of this error on the results presented is discussed in section 3.2.

## 2.4 Spatial data generation

Digital Surface Models (DSMs) and orthomosaics were created by application of SfM techniques (Westoby et al., 2012) using the software Postflight Terra 3D, which was provided with the UAV. Default settings likely resulted in overexposed pixels, which created erroneous points in the point cloud over snow that appeared several metres above the real snow surface. This issue could partly be solved with a semi-global-matching option within the software, which reduced the number of affected areas. Remaining areas with errors were manually excluded (Harder et al., 2016). DSMs and orthomosaics were resampled to a common grid and resolution of 10 cm, which increased the speed of subsequent data analysis substantially.

Subtracting DSMs provided both snow depth (HS) and differences in snow depth (dHS). dHS was scaled by the time interval between observations for comparison of varying observation periods. Snow covered area (SCA) was defined using individual thresholds in RGB values for different flights using the orthomosaics. Manual adjustment was needed to ensure that very dark snow was classified correctly (see for example Fig. 3b). HS was masked by the SCA of the date of the flight, whilst dHS was masked by the SCA on the dates of the first and subsequent flight. Figure 3c and 3d show examples of HS and dHS maps of a part of the study area. Several areas such as ski lifts and snow cat tracks and erroneous points as mentioned above were excluded from the analysis. Furthermore, large errors were detected in areas close to vegetation, which were manually excluded. The marked green area in Fig. 3d indicates the excluded area for this part of the study area.

To explain the observed differences in snow depth, several topographical variables were created using the DSMs. *Deviation from North* and *Slope* were calculated on a 1 m resolution to exclude small-scale noise of the DSMs. *Solar Irradiance* was calculated for a 1 m resolution for each flight day with the Area Solar Radiation function in ArcGIS. To account for albedo differences the *Brightness* of the orthomosiac pixels was abstracted on a 10 cm resolution. The blue value was chosen since it was least affected by unwanted illumination differences due aspect variations. *Brightness* and *Solar Irradiance* are temporal averages based on the first and the last flight and, if available, flights within the periods.

## 2.5 Data analysis

To identify reasons for spatial differences in snow depth change (dHS), Pearson correlation coefficients were calculated with several potential explaining variables as *Slope*, *Deviation from North*, *Solar Irradiance*, *Brightness*, current snow depth (HS) and snow depth at the beginning of the study period (HS0). Scatter plots also were visually inspected to detect reasons for strong or weak correlations or non-linear dependencies. The scatter plots were too dense to interpret visually because of the high resolution and so instead of plotting point pairs, the density of point pairs in a limited area of the plot was visualized (e.g. in Fig. 5a).

In addition to this univariate analysis, a stepwise forward-backward linear regression was used to define a small subset of variables and to calculate the coefficient of determination $r^2$ and coefficients of normalized explaining variables. Regular tests for including or excluding variables in a regression will fail given the large number of data ($N > 10^5$). Instead, a threshold for an increase in $R^2$ of 0.2 was defined to include an additional variable. A variable was excluded for any increase of $R^2$.

Spatial dependencies of the spatial structure of dHS and its correlation with explaining variables were analysed with variograms and correlograms. Variograms were calculated with

$$\hat{\gamma}_x(h) = \frac{1}{2\,|N(h)|} \sum_{(i,j)\in N(h)} (x_j - x_i)^2 , \qquad (1)$$

Hydrol. Earth Syst. Sci. Discuss., https://doi.org/10.5194/hess-2018-254
Manuscript under review for journal Hydrol. Earth Syst. Sci.
Discussion started: 14 May 2018


for point pairs $x_i$ and $x_j$ in a lag distance class $N(h)$ (e.g. Webster and Oliver, 2007). Correlations between two variables $x$ and $y$ in a certain lag distance $h$ were calculated with the cross-variogram as an estimator of the covariance (Webster and Oliver, 2007).

$$\hat{\gamma}_{xy}(h) = \frac{1}{2|N(h)|} \sum_{(i,j)\in N(h)} (x_j - x_i)(y_j - y_i) , \qquad (2)$$

This covariance was scaled with estimators of the variance $\hat{\gamma}_x$ (Eq. 1) using

$$\rho_{xy}(h) = \frac{\hat{\gamma}_{xy}(h)^2}{\hat{\gamma}_x(h)\hat{\gamma}_y(h)}, \qquad (3)$$

to obtain a correlation measure (Webster and Oliver, 2007). Variograms and correlograms were calculated only with a random subset of 10% of available data points to save computational resources. Smallest number observations were N > $5x10^4$, which was large enough to obtain consistent variograms and correlograms with different randomly chosen subsets.

# 3 Results and discussion

## 3.1 Overview and meteorology

Fortress Ridge is well exposed to the wind with peak hourly wind speeds over 20 m/s and a mean of 4.6 m/s over the winter 2014/15 at the FRG station. Two dominant wind directions can be identified, WSW and ESE, the latter is approximately perpendicular to the ridge. The wind direction parallel to the ridge is associated with the highest wind speeds. During precipitation and high wind events both directions were frequent. During late melt in 2015, wind speeds were substantially lower with a higher frequency of very calm days, providing more frequent flying conditions for the UAV.

Due to high wind speeds, large parts of the ridge were snow free during most of the exceptionally warm and dry winter season. After a large late November 2014 snow storm, the FRG station rarely documented snow on the ground and shallow snowpacks that did form were regularly eroded by wind within a few days. The snow covered area (SCA) reached the seasonal maximum in late November after this substantial snowfall (80 mm) with light winds

Hydrol. Earth Syst. Sci. Discuss., https://doi.org/10.5194/hess-2018-254
Manuscript under review for journal Hydrol. Earth Syst. Sci.
Discussion started: 14 May 2018



and dropped dramatically due to subsequent wind redistribution from blowing snow storms. When aerial measurements began on 19 May 2015, SCA was slightly below its typical winter value as spring ablation was under way. Without excluding any areas (see section 2.4) SCA was approximately 0.45 in both subareas (Fig. 3a).

Dust-on-snow was an obvious feature in late winter and the beginning of the melt season (Fig. 3b). It has not been observed to such extent in over a decade of observations in the region. This dust was locally eroded from the fine frost-shattered and saltation-pulverized shale particles at the ridge-top and was transported by wind to adjacent lee slopes and into gullies, similarly to wind-transported snow. Hence dust was deposited preferentially to snow drifts. Subsequent snow accumulation and melt processes led to a dust-on-snow pattern of high small-scale variability. The lower albedo from dust deposition may have influenced snowmelt energetics, but its high variability is different from the large scale, areally uniform dust deposition reported by Painter et al. (2010) where the dust source is in upwind arid zones and very fine aerosols are evenly deposited on snow.

Blowing snow transport during the high wind speeds also caused a highly variable snow depth (Fig. 3c) as is expected in the region (MacDonald et al., 2010; Pomeroy et al., 2012; Musselman et al., 2015). Snow was redistributed to the SE facing slopes of the ridge and also in gullies on the NW facing slopes, which are perpendicular to the ridge. Areas of bare ground and very deep snow (> 4 m) were only separated by a few metres distance. This high variability of snow depth at scales of from a few to tens of metres is a typical feature for wind-swept alpine snow covers (e.g. Pomeroy and Gray, 1995, p.22-27; Deems et al., 2006; Trujillo et al., 2007; Schirmer et al., 2011; Schirmer and Lehning, 2011).

An example of reductions in snow depth (dHS) due to ablation over a period of 13 days is shown in Fig. 3d. At the first glance differences between aspects are obvious, as well as smaller scale impact of albedo variations (cf. Fig. 3b). The driving forces to differences in ablation inferred from the observed differences in depth change will be examined in section 3.3.

The study period covered the late melt period, when the highest ablation rates occurred. Peak SWE of 500 mm was measured with a weighing snow lysimeter (Sommer "Snow Scale") in a nearby forest clearing on 20 April 2015. By the start of the study period on 19 May, SWE had gradually decreased to 300 mm, often interrupted by snowfall. During the study period after 19 May no significant (>3 cm) snowfall was observed. The much higher

Hydrol. Earth Syst. Sci. Discuss., https://doi.org/10.5194/hess-2018-254
Manuscript under review for journal Hydrol. Earth Syst. Sci.
Discussion started: 14 May 2018


ablation rates compared to the previous weeks caused the snow to disappear at this station on 30 May. A very similar development could be observed at two other stations using snow depth sensors within the Fortress Mountain Snow Observatory, including the FRS station (c.f. Fig. 2a). On 30 May a SCA of 0.2 was measured from the UAV over the whole flight domain. Considering a typical pre-melt SCA of approximately 0.45, the presence of a significant SCA illustrates the value of spatially distributed measurements of snow ablation and cover, when all seven meteorological stations in the ~3 km$^2$ region were snow-free.

A meteorological overview during the study period is given in Fig. 4 at the FRG station (cf. Fig. 2a). Measurements of incoming shortwave radiation and air temperatures are shown on the left, and resulting modelled results with SNOBAL in CRHM (cf. Fang et al., 2013) for a flat field simulation on the right. Although the FRG station was snow-free, CRHM was initialized with a hypothetical SWE amount of 800 mm in order to represent deeper nearby snow patches. Energy fluxes were summed and scaled for comparison over the indicated dates with UAV flights. The energy balance was dominated by inputs of net shortwave radiation. Melt accelerated around 8 June when high incoming shortwave radiation was accompanied by smaller longwave radiation losses and larger sensible heat fluxes driven by air temperatures often in excess of 10$^o$ C.

### 3.2 Selection of melt periods

Melt periods were chosen to include sufficient ablation such that the signal of dHS exceeded the measurement error from the UAV and data processing. A signal-to-noise ratio (SNR) was used, which relates the mean dHS with the typical standard deviation error (SD) found by Harder et al. (2016) for surfaces measured with the UAV to be 6.2 cm. Since two surface measurements are needed to achieve a dHS map, this SD value was doubled. For SNR ≥ 4, the signal is assumed to be sufficiently large to avoid mistaking it for a fluctuation in noise (Rose, 1973). Applying this criterion, mean dHS had to be larger than ~0.5 m. This melt amount was reached when melt periods were longer than approximately eight days. Given the availability of suitable flights in both subregions, this permitted two time periods for analysis; P1 from 19 May to 01 June and P2 01 June to 24 June.

Hydrol. Earth Syst. Sci. Discuss., https://doi.org/10.5194/hess-2018-254
Manuscript under review for journal Hydrol. Earth Syst. Sci.
Discussion started: 14 May 2018


### 3.3 Spatial differences in dHS

Table 1 shows the Pearson's correlation coefficient for above mentioned melt periods and different subareas. This univariate analysis shows clearly two driving factors for the earlier melt period, P1, albedo and solar radiation differences, expressed respectively with *Brightness* and either *Deviation from North* or with *Solar Irradiance* (Table 1). The sign of the correlations is mainly as expected: More southerly and darker pixels melted faster. Exceptions (e.g. during P2 in the southern subarea) may be explained with observable differences between a few remaining snow patches with different albedo values, slope, snow depths and sky view factors. Energy contributions from longwave radiation (DeBeer and Pomeroy, 2009) or altered turbulent heat fluxes because of cold air pooling (Mott et al., 2011; 2016) may override an obvious relationship with solar radiation. Also, faster settling rather than melt of deeper snowis possible, although the snowpack is quite ripe at this time of the year.

In the first period, P1, *Brightness* had a large effect in the northern subarea (r = -0.66). Figure 5a visualizes this relationship between dark snow and melt. The high scatter especially for brighter snow pixels can partly be explained with radiation differences. For the same period and area *Solar Irradiance* and *Deviation from North* had a correlation of r = 0.57. Figure 5b illustrates the dependency with *Solar Irradiance* but for white pixels only (approximately 50% of the observations). A clear dependency is visible with a correlation coefficient of r = 0.66. Radiation effects were more substantial during P2 in this northern subarea with r = 0.84 for both *Solar Irradiance* and *Deviation from North*. This may be explained due to less scatter produced by albedo differences in this period (r = 0.03). Darker parts of the snowcover melted out by the end of this period.

The correlations with *Brightness*, *Deviation from North* and *Solar Irradiance* were often strong. dHS increased from 5 to 7 cm/d (nearly 60% increase) as aspect shifted about 115 deg from north to south or snow from clean to dusty (c.f. Fig. 5). This shows the importance of spatial variation in net solar irradiance to melt energetics – as exemplified by the model energy budget shown in Fig. 4b. The impact of dust on albedo and slope on solar irradiance is well established in the snow literature and so this is expected. What is a more unique finding here is that dHS is not correlated largely with initial SWE (HS0, Table 1) as found by DeBeer and Pomeroy (2009, 2010), Pomeroy et al. (2003, 2004), Dornes et al. (2008 a, b) and other mountain studies in Canada. This indicates a lack of covariance between melt

Hydrol. Earth Syst. Sci. Discuss., https://doi.org/10.5194/hess-2018-254
Manuscript under review for journal Hydrol. Earth Syst. Sci.
Discussion started: 14 May 2018


rate and SWE in late melt that should have important implications for SCD curves (Pomeroy et al., 2001, section 3.4.3).

All previous studies in the Canadian Rockies, Alberta and Coast Mountains, Yukon focussed on the full melt period rather than the late melt period that is measured in this study and so the importance of season differences in irradiance to slopes as shown in Fig. 1 and the late-melt isothermal snowpacks may be important to explaining the missing spatial correlation between melt and SWE. During early melt the cold content is related to snow depth, which likely will result in a spatial correlation between SWE and melt (c.f. DeBeer and Pomeroy, 2010, 2017). Furthermore, the observed two dominant wind directions related to precipitation and strong wind speeds have influenced spatial SWE patterns and reduced the likelihood of a spatial correlation of SWE and melt. In contrast, areas with wind transport from primarily one direction and hence preferential SWE loading onto slopes will affect particular aspects, which in turn may be southerly, and hence induce a spatial correlation between SWE and ablation. Another reason for a missing spatial correlation is discussed in section 3.5, in which the mismatch of scales of ablation and SWE patterns are discussed.

The stepwise linear regression results shown in Table 2 confirm that the most important variables explaining ablation variation are solar irradiance and albedo. Combinations of solar irradiance and albedo increased the explanation compared to univariate regressions (Table 1). For example for P1 in the northern subarea, a model with *Deviation from North* and *Brightness* explained nearly 70% of the total ablation variance with nearly equally large (normalized) coefficients, indicating equal effect contributions of irradiance and albedo to explaining variations in dHS.

## 3.4 Relative importance of ablation and initial SWE

### 3.4.1 Variability of ablation in relation to (initial) SWE

Table 3 shows mean, standard deviation and CV values of HS and dHS in different periods and subareas. Throughout the melt season CV values of dHS were smaller than those of HS. At the start of the study period, the variability of dHS was smaller than that of HS by a factor 3.7 to 6.7, for the whole area approximately by a factor 5. Applying the mean measured snow density from 19 measurements between 19 May and 22 May (413 kg/m$^3$) to HS provides an estimate of mean initial SWE of 520 mm with a standard deviation of over 480 mm. Ablation amounts in period P1 were in mean 334 mm, with a standard deviation of only

65 mm. These values indicate much larger SWE variability than ablation variability in this period.

### 3.4.2 Persistence of ablation patterns

For the whole area only a weak correlation (r = 0.36) was found between ablation patterns between the long periods P1 and P2. Larger correlations were found for the northern subarea (r = 0.60). Ablation patterns in certain sub-periods with similar weather conditions were correlated to each other. For instance, ablation patterns in the cool and cloudy period between 05 May and 01 June were correlated with two other rather cloudy sub-periods at the end of the study period with r = 0.49 and r = 0.64, and to the later combined period P2 (r = 0.70). Closer investigations to weather conditions were not possible given the reduced signal-to-noise ratio for shorter time periods. Larger periods always included several types of weather patterns.

### 3.4.3 Depletion curves

Maximum differences in melt rate of up to 100% were measured (section 3.3) and melt rates were spatially persistent especially in the northern subarea. Similarly to Pomeroy et al. (2001) and Egli et al. (2012) the impact of spatial melt rates on snow-cover depletion and areal melt were analysed in several scenarios:

1. Variable HS0/uniform melt: This scenario started with the measured distribution of HS at the start of the study period (HS0) and a spatially uniform melt rate was applied for each pixel. This melt rate was determined with observed mean values shown in Table 3. Each pixel was reduced by this mean melt rate and any negative values in HS were set to 0. SCA was defined as the ratio of the number of grid points with HS > 0 to all pixels.
2. Uniform HS0/variable melt: In this scenario mean initial snow depth as shown in Table 3 was uniformly distributed in the whole snow-covered area. Spatially variable melt rates as measured with the UAV were applied to each pixel. To obtain the exact melt out time this scenario was calculated in a daily resolution with using a temporally constant melt rate between flights. No exact melt amounts are available for pixels which have melted out between flights. For those pixels the mean melt rate were applied. The general shape of SCD curves can be obtained when this scenario is also calculated on the time resolution of the UAV flights.

Hydrol. Earth Syst. Sci. Discuss., https://doi.org/10.5194/hess-2018-254
Manuscript under review for journal Hydrol. Earth Syst. Sci.
Discussion started: 14 May 2018

Hydrology and Earth System Sciences
Discussions

3. Uniform HS0/uniform melt: Similar to scenario 2, but a spatially uniform melt rate was applied to each pixel. This scenario was also calculated on a daily resolution.

In all scenarios SCA was set to 1 for the area which was snow-covered at the start of the study period. Figure 6 shows mean HS ablation and SCD curves for the whole area and the northern subarea (top), for which more flights are available. Differences between measured development and the first scenario of uniform melt and variable HS0 were not large. However, a large difference between measurements and the second and third scenario of uniform HS0 with either variable or uniform melt is obvious. Areal melt in those scenarios was overestimated before modelled melt out because of overestimating of SCA. Later during melt, areal melt was underestimated (or zero) since nearly (or all) snow disappeared too early. This is particularly important when the aim is to model late rain-on-snow events in hydrological models. For this area these results indicate that it is possible ignoring spatial melt variability in late melt to achieve a realistic SCD curve, while this is not possible ignoring spatial HS0 variability. This main feature is consistent with Egli et al. (2012).

The main reason why observed substantial and partly persistent melt differences were not largely influencing depletion curves compared to a homogeneous melt scenario can be found in the small or missing spatial correlation between melt and initial SWE (cf. section 3.3 and Table 1). Large correlations substantially influence SCD: Negative correlation accelerates SCD at the beginning of melt and delays it in late melt lengthening the snowmelt season and vice versa with positive correlations (Essery and Pomeroy, 2004).

In case of weak to no correlation, spatial melt differences can be quite large without affecting SCD curves compared to homogeneous melt. The spatially variable melt can be viewed as a nearly random process. There is still some impact because of the log-normal frequency distribution of SWE. Here, with a much larger variability of SWE compared to melt (see section 3.4.1) and only small correlations (see Table 1), SWE must dominate SCD.

### 3.5 Scale dependencies of melt

Figure 7 and 8 show how the variance of dHS, the variance of explaining variables and correlations thereof, develop with larger lag distance between point pairs (variograms and correlograms, Eqs. 1 to 3). This gives further insights into the driving factors of ablation and why a correlation between dHS and initial HS0 was weak in this study area during late melt.

In Fig. 7a shows with the variogram of dHS that the variance increased over two distinct length scales, one less than 50 m and one greater than 200 m. This implies that driving forces to generate variance for ablation need to be searched at these two scales. In section 3.3 a strong correlation was found between dHS and *Brightness* and *Solar Irradiance*, but only small correlations to HS0. These variables were also analysed with variograms and correlograms.

The variogram of *Brightness* shown in Fig. 7b indicates a variance increase only at the small lag distances less than 50 m. This is consistent with the visual impression of a small-scale variability of albedo shown in Fig. 3b. The correlogram shown in Fig. 7c reveals a strong correlation of *Brightness* with dHS at these small scales ($\rho_{xy} \approx -0.6$ at 50 m lag distance). This demonstrates that albedo was largely responsible for the small-scale melt variability observed in Fig. 7a.

Figure 8a shows the variogram of *Solar Irradiance*. A small increase for length scales less than 100 m suggests radiation and aspect differences at those scales (within-slope variations), but the largest increase can be observed at lag distances longer than 200 m. This scale represents slopes on both sides of the ridge and coincides with the larger scale of melt variance. Indeed, the correlogram (Fig. 8b) confirms that the largest correlation with melt to $\rho_{xy} = 0.4$ was achieved at those larger distances.

The same analysis for initial snow depth (HS0) can be seen in Fig. 8c and d. Most of the variance for snow depth is at length scales less than 100 m. The periodic behaviour shown beyond that scale may be due to the patchy snow cover which has long snow-free patches. No large correlation with dHS is observable on all scales (Fig. 8d).

This analysis offers an explanation why ablation and initial SWE were not correlated in these observations. Melt variance (ignoring the small-scale influence of albedo) was related to large scale aspect changes on both slopes, while snow depth was mainly variable at much smaller scales. This scale mismatch prevented a stronger correlation.

### 3.6 Comparison with other studies in alpine terrain

The correlation coefficients between dHS and explaining variables found here are larger than those found by Grünewald et al. (2010) in a Swiss alpine catchment. They found maximum correlations of $|r| \approx 0.4$ for altitude, slope, northing and initial SWE, mainly for the first of their ablation periods. This is despite the fact that they used a wider range of explaining variables such as wind fields from a high resolution wind flow model and accounted for time-variant diffuse radiation in modelling shortwave irradiance. The lower relation to explaining variables may be caused by regional differences, but can also be found in the slightly larger area (0.6 km$^2$) studied by Grünewald et al. (2010), which can potentially include more effects. These local effects were observable in our study as correlations change strength and sign with time and space (c.f. Table 1). Grünewald et al. (2010) found correlations diminished with time and explained this by suggesting the increasing importance of local advection of heat. These diminishing correlations were not observed here. They also found more similar variance in ablation and SWE. This may be explained by the particularly wind-swept study site.

Egli et al. (2012) working in the same catchment as Grünewald et al. (2010) found that SCD curves were insensitive to the degree of heterogeneity of ablation. This can be explained as they also did not find a large correlation between SWE and melt. As also found here, Egli et al. (2012) observed that when correlations developed, they were temporally and spatially unsteady, disappeared or changed sign. This reduced the impact of these small-scale correlations on SCD over the ablation season in within a larger study area.

In a northern Canadian mountain basin (Yukon), Pomeroy et al. (2004) observed on their smallest scale (100 to 300 m) a large negative correlation between ablation and SWE of r = -0.95 at the valley bottom part of their 660 m long transect, a correlation of r = -0.63 on the south face and no correlation on the north face slopes (c.f. their Fig. 5). This is in agreement to findings here that correlations vary regionally. Pomeroy et al. (2004) explained those differences with by varying exposures of vegetation, which is not a factor in this study. When these three slopes are aggregated to the sub-basin, the areal multi-scale correlation is diminished (Fig. 5, Pomeroy et al., 2004). The large correlation of r = -0.86 over the sub-basin is driven by a slope-scale association between snow redistribution to north faces that also experience lower ablation rates (Fig. 6, Pomeroy et al., 2004). This is a meso-scale feature of southerly winds in the basin due to proximity of the Pacific Ocean to the south. Dornes et al. (2008) showed that representing differences in ablation rates amongst these slopes is critical to calculating accurate SCD, but did not suggest that small-scale ablation rate variation need to be considered. They found that by disaggregating the basin into slope units with averaged melt energy applied to each unit, then accurate SCD curves could be estimated within each slope unit using the variability of SWE alone.

Hydrol. Earth Syst. Sci. Discuss., https://doi.org/10.5194/hess-2018-254
Manuscript under review for journal Hydrol. Earth Syst. Sci.
Discussion started: 14 May 2018

Hydrology and Earth System Sciences
Open Access
Discussions

DeBeer and Pomeroy (2010; 2017) concluded that multi-scale variable melt and SWE improved SCD modelling compared to aerial photography of SCA during early melt, but not mid or late melt seasons in the Canadian Rockies (Marmot Creek Basin). They included a spatial distribution of SWE within four slope-scale subareas, and modelled the cold content of snow, which introduced an early multi-scale correlation between SWE and melt in the model. Applying different melt rates within each of the slope-based subareas improved simulations of SCD compared to uniform melt rates during early melt. Considering the whole ablation season they concluded that "…the improvements from including simulations of inhomogeneous melt over the entire snowmelt period in the spring were negligible (Table 3)." This refers to small scale inhomogeneous melt and is in agreement with the measurements presented here. Over Fisera Ridge in the same region, Musselman et al. (2015) showed a slope-scale but not fine-scale spatial association between ablation and SWE, and noted that the slope scale association was due to the localized wind-loading of this particular ridge (northerly winds) and would not apply to the larger basin studied by DeBeer and Pomeroy (2017) or Pomeroy et al. (2016) where wind directions varied.

Winstral and Marks (2014) found modelled SWE and melt rates were correlated with $r = -0.66$. This large modelled correlation of spatial patterns of SWE and melt may be realistic in this study area, since snow transport is dominated there by a rather homogeneous wind direction, both in space and time which leads to a coincidence between preferentially loaded slopes and melt energy. Such a large correlation between modelled melt and SWE would indicate that spatial melt differences are relevant to model SCD correctly in this area.

In summary, some studies found correlations between melt and SWE at slope scales, but not at fine scales. These associations were strongest early in melt and at higher latitudes and where wind redistribution occurred over consistent directions due to synoptic conditions during mesoscale wind loading of slopes and is consistent with the slope-based solar irradiance differences shown in Fig. 1. However, no study showed consistent and persistent fine-scale association between ablation and SWE suggested that they can be considered uncorrelated in modelling at fine scales. To address differences in melt energy at slope scales, modellers can chose to calculate averaged energetics to slope units and apply a mean ablation rate to a frequency distribution of SWE over the slope as was demonstrated by Dornes et al. (2008) and DeBeer and Pomeroy (2010; 2017). This is computationally more efficient than the fully distributed calculations employed by Winstral and Marks (2014) and Musselman et al. (2015) and is a promising and likely necessary direction for disaggregation of land surface schemes calculations of melt in mountain regions.

## 4 Conclusions and outlook

The aim of this study was to determine factors which influence areal snow ablation patterns in alpine terrain. The dependency of SWE and topographic variables on spatial melt rates were analysed for an alpine ridge in the Fortress Mountain Snow Laboratory located in the Canadian Rocky Mountains. Detailed maps of snow depth (HS), snow depth changes (dHS) and snow-covered area (SCA) were generated during late season ablation with UAV based orthophotos, photogrammetry and Structure-from-Motion techniques. HS and dHS served as proxies for SWE and melt rates. Ablation rates were found to be spatially variable and mainly dependent on variation in solar irradiance and albedo. Local and small-scale dust variations, which have never been observable to this degree in the area, increased the variability of ablation.

However, snow-cover depletion (SCD) curves were largely dominated by the SWE variability at the start of this study, which was approximately five times larger than melt variability in this extraordinarily windswept environment. More importantly, SWE and melt rates were not strongly correlated over space, which is a prerequisite for melt influencing SCD. Three reasons for lack of spatial association between ablation and SWE patterns here are: (1) the snowcover was isothermal during of the study period so that spatial differences in the depth dependent cold content as found by DeBeer and Pomeroy (2010), did not play a relevant role; (2) the SWE pattern was influenced by two dominating wind directions, preventing wind loading on particular slopes coincident with either larger or low energy input as found by Pomeroy et al. (2003), Dornes et al. (2008 a,b) and Musselman et al. (2015); (3) near summer solstice conditions limited differences of radiation energy input between slopes; (4) a scale mismatch between the variabilities of ablation and SWE was detected, with SWE varying mostly on smaller scales (in-slope gullies, ridges), while melt varied mostly on larger slope-scale aspect differences.

These findings suggest that during those conditions SCD curves can be calculated without the spatial distribution of melt rates, while hydrological and atmospheric models need to implement a realistic distribution of SWE in order to do this. Comparison of these results to those found in Switzerland, Yukon, the Canadian Rockies and mountains in Idaho, indicates

Hydrol. Earth Syst. Sci. Discuss., https://doi.org/10.5194/hess-2018-254
Manuscript under review for journal Hydrol. Earth Syst. Sci.
Discussion started: 14 May 2018



that clear advice to modellers is still not possible. It is not possible to determine without detailed modelling or measurements whether, when and where a catchment-wide multi-scale association between SWE and melt are capable to sufficiently alter SCD curves from those derived with an uniform melt assumption.

Thus, longer time series of spatially detailed SWE observations need to be made in order to further test and examine the spatial covariance and variance of ablation and SWE in order to suggest how to efficiently and accurately model snow-cover depletion and runoff in snow-melt dominated catchment, and to deal with region variations in associations between SWE and melt, without relying on powerful calibration routines. This will help to transfer snow-hydrological models to ungauged catchments and to model future scenarios.

## 5 Data availability

The data is available, upon request from the database manager (Branko Zdravkovic), in the Changing Cold Regions (CCRN) dataserver. (www.ccrnetwork.ca/outputs/data/index.php). Please refer to this website for contact details. The data involves all UAV derived grids for HS, dHS and SCA, as well as grids of explaining variables (Brightness, Deviation from North and Slope) in 1 m resolution (cp. section 2.4). Metadata is provided which explains the file naming convention of the grids (dates and variables).

## 6 Acknowledgement

The authors wish to acknowledge Phillip Harder for UAV training, Chris Marsh for post-processing and modelling support, May Guan and Angus Duncan for extensive field work help, Xing Fang for the assistance in modelling CHRM results, as well as Phillip Harder, Jonathan Conway, Keith Musselman, Nico Leroux and Nik Aksamit for and helpful comments and discussions. We are grateful for logistical support from Fortress Mountain Ski Resort, Cherie Westbrook for access to a differential GPS unit. Funding was provided by NSERC through Discovery and Research Tools and Instruments grants and NSERC's Changing Cold Regions Network, by the Canada Research Chairs and Canada Excellence Research Chairs programmes and by Alberta Agriculture and Forestry.

## 7 References

Anderton, S. P., White, S. M., & Alvera, B. (2004). Evaluation of spatial variability in snow water equivalent for a high mountain catchment. Hydrological Processes, 18(3), 435-453.

DeBeer, C. M., & Pomeroy, J. W. (2009). Modelling snow melt and snowcover depletion in a small alpine cirque, Canadian Rocky Mountains. Hydrological processes, 23(18), 2584-2599.

DeBeer, C. M., & Pomeroy, J. W. (2010). Simulation of the snowmelt runoff contributing area in a small alpine basin. Hydrology and Earth System Sciences, 14(7), 1205.

DeBeer, C. M., & Pomeroy, J. W. (2017). Influence of snowpack and melt energy heterogeneity on snow cover depletion and snowmelt runoff simulation in a cold mountain environment. Journal of Hydrology, 553, 199-213.

Deems, J. S., Fassnacht, S. R., & Elder, K. J. (2006). Fractal distribution of snow depth from LiDAR data. Journal of Hydrometeorology, 7(2), 285-297.

Donald, J. R., Soulis, E. D., Kouwen, N. & Pietroniro, A. (1995). A Land Cover-Based Snow Cover Representation for Distributed Hydrologic Models. Water Resources Research, 31, 995-1009.

Dornes, P. F., Pomeroy, J. W., Pietroniro, A., Carey, S. K. & Quinton, W. L. (2008a). Influence of landscape aggregation in modelling snow-cover ablation and snowmelt runoff in a sub-arctic mountainous environment. Hydrological Sciences Journal, 53, 725-740.

Dornes, P. F., Pomeroy, J. W., Pietroniro, A. and Verseghy, D. L. (2008b): Effects of spatial aggregation of initial conditions and forcing data on modeling snowmelt using a land surface scheme. Journal of Hydrometeorology, 9, 789-803.

Egli, L., Jonas, T., Grünewald, T., Schirmer, M., & Burlando, P. (2012). Dynamics of snow ablation in a small Alpine catchment observed by repeated terrestrial laser scans. Hydrological Processes, 26(10), 1574-1585.

Essery, R., & Pomeroy, J. (2004). Implications of spatial distributions of snow mass and melt rate for snow-cover depletion: theoretical considerations. Annals of Glaciology, 38(1), 261-265.

Fang, X., Pomeroy, J. W., Ellis, C. R., MacDonald, M. K., DeBeer, C. M., & Brown, T. (2013). Multi-variable evaluation of hydrological model predictions for a headwater basin in the Canadian Rocky Mountains. Hydrology and Earth System Sciences, 17(4), 1635-1659.

Faria, D. A., Pomeroy, J. W. and Essery, R. L. H. (2000): Effect of covariance between ablation and snow water equivalent on depletion of snow-covered area in a forest. Hydrological Processes, 14, 2683-2695.

Grünewald, T., Schirmer, M., Mott, R., & Lehning, M. (2010). Spatial and temporal variability of snow depth and ablation rates in a small mountain catchment. Cryosphere, 4(2), 215-225.

Harder, P., Schirmer, M., Pomeroy, J. & Helgason, W. (2016). Accuracy of snow depth estimation in mountain and prairie environments by an unmanned aerial vehicle. The Cryosphere, 10, 2559-2571.

Kuchment, L. & Gelfan, A. (1996). The determination of the snowmelt rate and the meltwater outflow from a snowpack for modelling river runoff generation. Journal of Hydrology, 179, 23 - 36.

Luce, C. H., Tarboton, D. G., and Cooley, K. R. (1998). The influence of the spatial distribution of snow on basin-averaged snowmelt. Hydrological Processes, 12, 1671-1683.

Luce, C. H., Tarboton, D. G., and Cooley, K. R. (1999): Sub-grid parameterization of snow distribution for an energy and mass balance snow cover model. Hydrological Processes, 13, 1921–1933.

MacDonald, M. K., Pomeroy, J. W. & Pietroniro, A. (2010). On the importance of sublimation to an alpine snow mass balance in the Canadian Rocky Mountains. Hydrology and Earth System Sciences, 14, 1401-1415.

Magnusson, J., Farinotti, D., Jonas, T., & Bavay, M. (2011). Quantitative evaluation of different hydrological modelling approaches in a partly glacierized Swiss watershed. Hydrological Processes, 25(13), 2071-2084.

Marks, D., & Dozier, J. (1992). Climate and energy exchange at the snow surface in the alpine region of the Sierra Nevada: 2. Snowcover energy balance, Water Resources Research., 28, 3043-3054.

Marsh, P. and Pomeroy, J. W. (1996). Meltwater fluxes at an arctic forest-tundra site. Hydrological Processes, 10, 1383-1400.

Ménard, C. B., Essery, R. and Pomeroy, J. (2014). Modelled sensitivity of the snow regime to topography, shrub fraction and shrub height. Hydrology and Earth System Sciences, 18, 2375-2392.

Mott, R., Egli, L., Grünewald, T., Dawes, N., Manes, C., Bavay, M., & Lehning, M. (2011). Micrometeorological processes driving snow ablation in an Alpine catchment. The Cryosphere, 5(4), 1083-1098.

Mott, R., Gromke, C., Grünewald, T., & Lehning, M. (2013). Relative importance of advective heat transport and boundary layer decoupling in the melt dynamics of a patchy snow cover. Advances in Water Resources, 55, 88-97.

Mott, R., Paterna, E., Horender, S., Crivelli, P. & Lehning, M. (2016). Wind tunnel experiments: cold-air pooling and atmospheric decoupling above a melting snow patch. The Cryosphere, 10, 445-458.

Musselman, K. N., Pomeroy, J. W., Essery, R. L. H. & Leroux, N. (2015). Impact of windflow calculations on simulations of alpine snow accumulation, redistribution and ablation. Hydrological Processes, 29, 3983-3999.

Painter, T. H., Deems, J. S., Belnap, J., Hamlet, A. F., Landry, C. C., & Udall, B. (2010). Response of Colorado River runoff to dust radiative forcing in snow. Proceedings of the National Academy of Sciences, 107(40), 17125-17130.

Pohl, S., Marsh, P. & Liston, G. (2006). Spatial-temporal variability in turbulent fluxes during spring snowmelt. Arctic, Antarctic, and Alpine Research, 38, 136-146.

Pomeroy, J., & Gray, D. (1995). Snowcover-accumulation, relocation and management. National Hydrology Research Institute Science Report No. 7. Saskatoon, Canada.

Pomeroy, J. W., Gray, D. M., Shook, K. R., Toth, B., Essery, R. L. H., Pietroniro, A. & Hedstrom, N. (1998). An evaluation of snow accumulation and ablation processes for land surface modelling. Hydrological Processes, 12, 2339-2367.

Pomeroy, J. W., Hanson, S., & Faria, D. (2001). Small-scale variation in snowmelt energy in a boreal forest: an additional factor controlling depletion of snow cover. In Proceedings of the Eastern Snow Conference, 58, 85-96.

Pomeroy, J. W., Toth, B., Granger, R. J., Hedstrom, N. R., & Essery, R. L. H. (2003). Variation in surface energetics during snowmelt in a subarctic mountain catchment. Journal of Hydrometeorology, 4(4), 702-719.

Pomeroy, J., Essery, R., & Toth, B. (2004). Implications of spatial distributions of snow mass and melt rate for snow-cover depletion: observations in a subarctic mountain catchment. Annals of Glaciology, 38(1), 195-201.

Pomeroy, J., Fang, X. and Ellis, C. (2012): Sensitivity of snowmelt hydrology in Marmot Creek, Alberta, to forest cover disturbance. Hydrological Processes, 26, 1891-1904.

Pomeroy J.W., Fang X. and Marks D.G. (2016): The cold rain-on-snow event of June 2013 in the Canadian Rockies - characteristics and diagnosis. Hydrological Processes, 30, 2899-2914. DOI: 10.1002/hyp.10905

Schirmer, M., & Lehning, M. (2011). Persistence in intra-annual snow depth distribution: 2. Fractal analysis of snow depth development. Water Resources Research, W09516.

Schirmer, M., Wirz, V., Clifton, A., & Lehning, M. (2011). Persistence in intra-annual snow depth distribution: 1. Measurements and topographic control. Water Resources Research, W09517.

Shook, K. & Gray, D. M. (1996). Small-scale spatial structure of shallow snowcovers. Hydrological Processes, 10, 1283-1292.

Skiles, S. M., Painter, T. H., Belnap, J., Holland, L., Reynolds, R. L., Goldstein, H. L. & Lin, J. (2015). Regional variability in dust-on-snow processes and impacts in the Upper Colorado River Basin. Hydrological Processes, 29, 5397-5413.

Trujillo, E., Ramírez, J. A., & Elder, K. J. (2007). Topographic, meteorologic, and canopy controls on the scaling characteristics of the spatial distribution of snow depth fields. Water Resources Research, 43(7).

Verseghy, D. L. (2000). The Canadian land surface scheme (CLASS): Its history and future. Atmosphere-Ocean, 38, 1-13.

Webster, R. and Oliver, M. (2007): Geostatistics for Environmental Scientists.

Westoby, M., Brasington, J., Glasser, N., Hambrey, M. & Reynolds, J. (2012): "Structure-from-Motion" photogrammetry: A low-cost, effective tool for geoscience applications, Geomorphology, 179, 300–314.

Winstral, A., & Marks, D. (2002). Simulating wind fields and snow redistribution using terrain-based parameters to model snow accumulation and melt over a semi-arid mountain catchment. Hydrological Processes, 16(18), 3585-3603.

Winstral, A., Marks, D., & Gurney, R. (2013). Simulating wind-affected snow accumulations at catchment to basin scales. Advances in Water Resources, 55, 64-79.

Winstral, A., & Marks, D. (2014). Long-term snow distribution observations in a mountain catchment: Assessing variability, time stability, and the representativeness of an index site. Water Resources Research, 50(1), 293-305.

Hydrol. Earth Syst. Sci. Discuss., https://doi.org/10.5194/hess-2018-254
Manuscript under review for journal Hydrol. Earth Syst. Sci.
Discussion started: 14 May 2018




## Figures

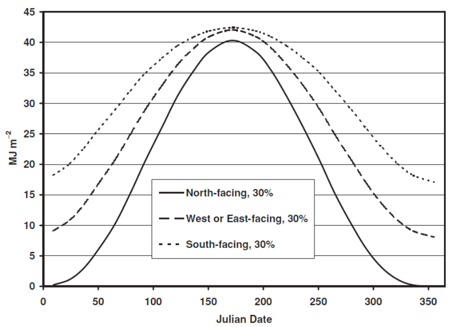


*Figure 1. Extraterrestrial solar irradiance at 50° N for north, south and east/west facing 30 % slopes. Note the small differences as summer solstice is approached (Male and Gray, 1981).*

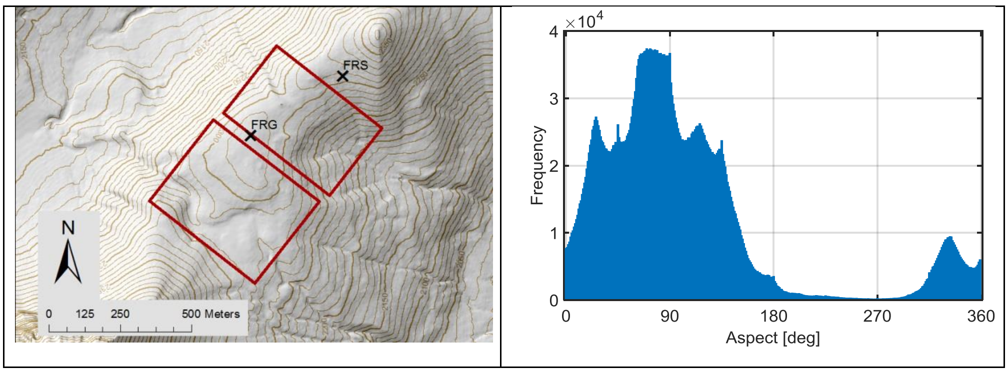


*Figure 2. Topography of the study site, (a) Overview of the two areas of investigation (red rectangles) with the location of the two weather stations (black crosses) on the alpine Fortress Ridge, Alberta, Canada, and (b) aspect distribution of the snow covered area at 27 May 2015 (spatial resolution of 10 cm, N > 3 x 10^6).*

Hydrol. Earth Syst. Sci. Discuss., https://doi.org/10.5194/hess-2018-254
Manuscript under review for journal Hydrol. Earth Syst. Sci.
Discussion started: 14 May 2018




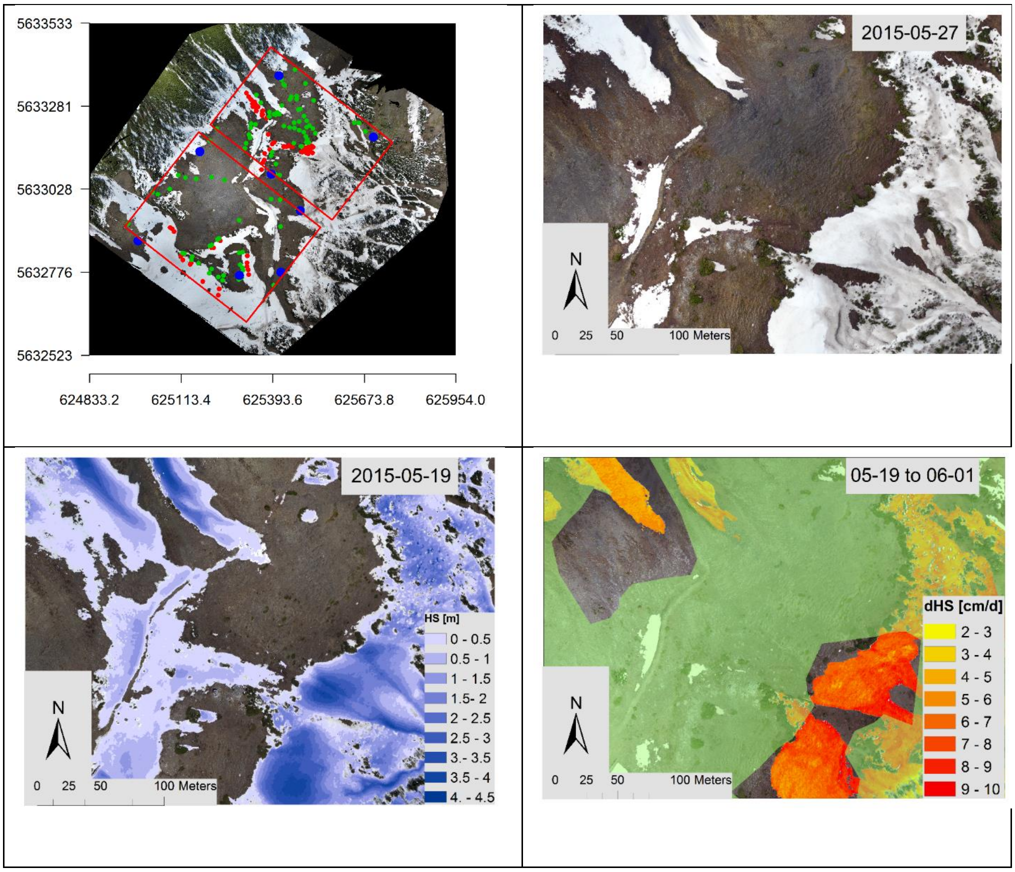


*Figure 3. UAV photogrammetric data for the study site: (a) orthomosaic from images captured on 22 May 2015, showing the two N and S areas of investigation (red polygons). Points indicate locations of manual snow depth and differential GPS measurements over snow (red) and bare ground (green). (B) enlargement of part of the study area showing evidence of dust on snow, (c) snow depth (HS) on 19 May 2015 and d) differences in snow depth (dHS) between that date and 1 June. The green colour in (d) indicates areas excluded from analysis because of human impacts on snow or substantive vegetation.*

Hydrology and Earth System Sciences
Discussions
Open Access

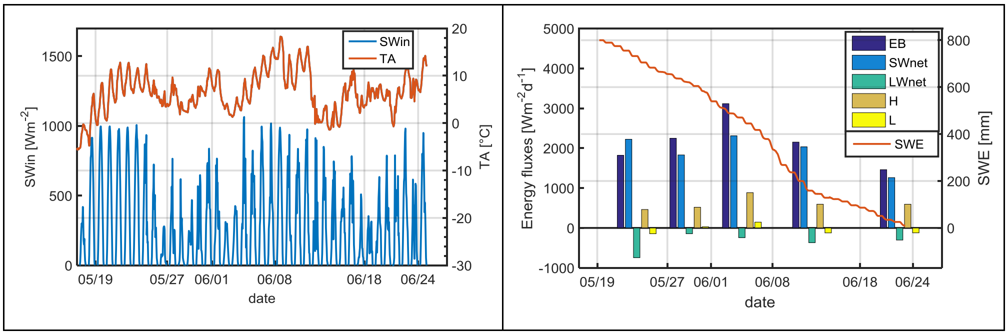


*Figure 4: Measured (a) and modelled (b) values at the FRG station, energy fluxes per day for periods between UAV flights as modelled by SNOBAL in CRHM. EB is the total energy flux, SWnet and LWnet are net shortwave and longwave radiation, H and L are sensible and latent heat fluxes. Heat advected by rain and ground heat flux, with only small contributions are not shown.*

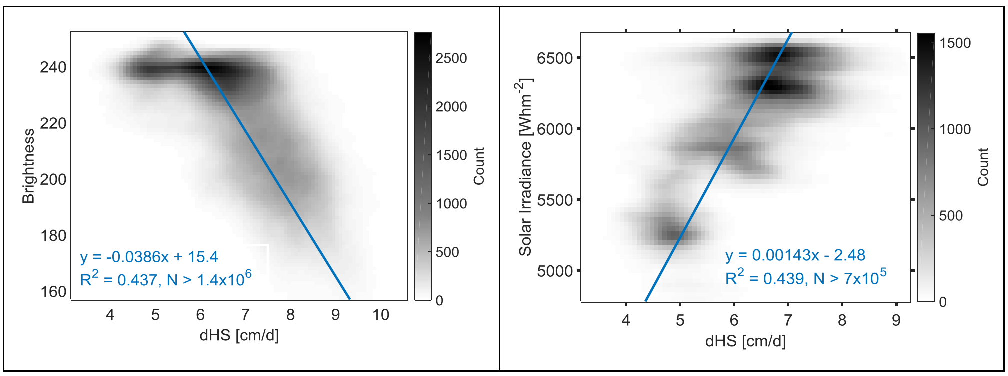


*Figure 5. Scatter plots of (a) snow brightness and b) solar irradiance versus differences in snow depth (dHS). Darker tones indicate a higher density of points. For (b) only bright snow pixels are used (brightness > 230). Blue lines indicate the linear regression lines, which are highly significant (p = 0) because of the large number of observations.*

Hydrol. Earth Syst. Sci. Discuss., https://doi.org/10.5194/hess-2018-254
Manuscript under review for journal Hydrol. Earth Syst. Sci.
Discussion started: 14 May 2018



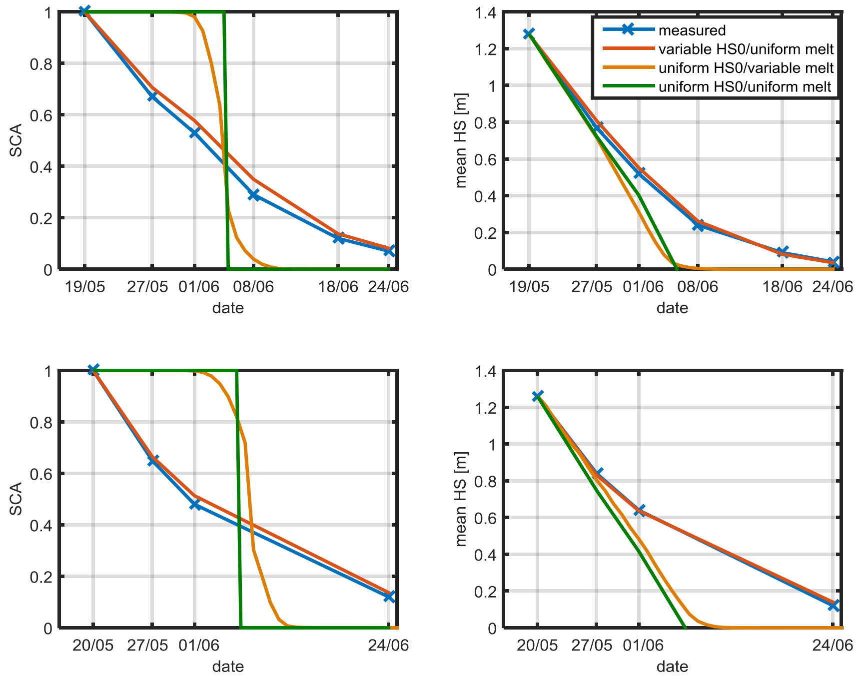


1
2 *Figure 6. SCD and mean HS ablation for subarea N (a, b) and the total area (c,d). Blue are measured*
3 *values, red are modelled values with initialized with measured HS distribution on May 19 and uniform*
4 *melt, green are modelled values initialized with uniform snow depth distribution and uniform melt.*

Hydrol. Earth Syst. Sci. Discuss., https://doi.org/10.5194/hess-2018-254
Manuscript under review for journal Hydrol. Earth Syst. Sci.
Discussion started: 14 May 2018

Hydrology and Earth System Sciences
Discussions

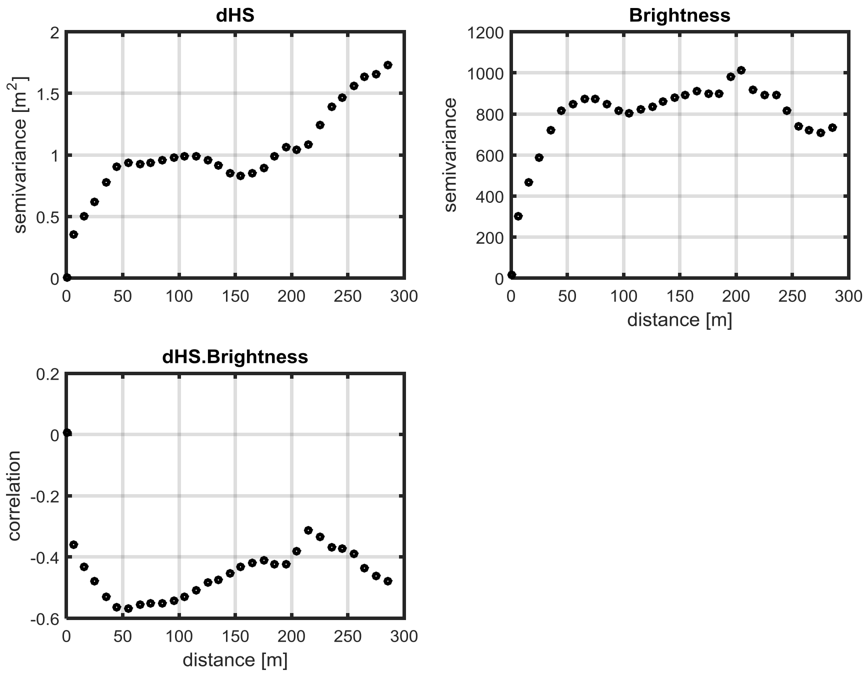


Figure 7. Variograms and correlogram for dHS and Brightness.

Hydrol. Earth Syst. Sci. Discuss., https://doi.org/10.5194/hess-2018-254
Manuscript under review for journal Hydrol. Earth Syst. Sci.
Discussion started: 14 May 2018



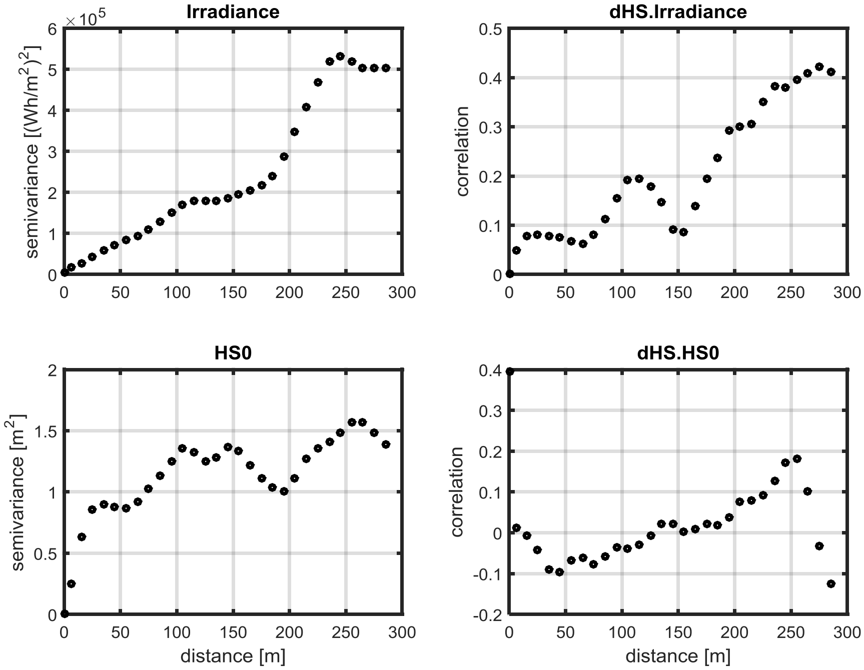


*Figure 8. Correlograms with dHS and variograms for initial HS0 and modelled Irradiance.*

Hydrol. Earth Syst. Sci. Discuss., https://doi.org/10.5194/hess-2018-254
Manuscript under review for journal Hydrol. Earth Syst. Sci.
Discussion started: 14 May 2018


Hydrology and Earth System Sciences
Open Access
Discussions

# Tables

*Table 1. Pearson's correlations coefficient r between dHS and explaining variables. P1 is from 19 May to 01 June and P2 from 01 June to 24 June. N is number of observations.*

| Period | Area | Brightness | Degrees from North | Solar Irradiance | HS0 | N |
|---|---|---|---|---|---|---|
| P1 | all | -0.47 | 0.56 | 0.39 | -0.12 | 3245837 |
| P2 | all | -0.59 | 0.30 | 0.01 | 0.33 | 706344 |
| P1 | N | -0.66 | 0.57 | 0.57 | -0.24 | 1410768 |
| P2 | N | 0.03 | 0.84 | 0.84 | 0.03 | 183822 |
| P1 | S | -0.43 | 0.39 | 0.33 | 0.01 | 1835069 |
| P2 | S | -0.68 | -0.21 | -0.61 | 0.30 | 522522 |

*Table 2. Results from stepwise linear regression. DegN stands for Degrees from North, Bright for Brightness, SolIrr for Solar Irradiance. Bright1 is the Brightness at the date of the first flight. The coefficients are normalized, which lead to negligible intercepts.*

| Period | Area | Regression equation | $R^2$ | N |
|---|---|---|---|---|
| P1 | all | dHS = 0.62·DegN - 0.54·Bright | 0.60 | 3245837 |
| P2 | all | dHS = 0.25·Slope + 0.41·DegN - 0.60·Bright | 0.52 | 706344 |
| P1 | N | dHS = 0.49·DegN - 0.59·Bright | 0.67 | 1410768 |
| P2 | N | dHS = 0.84·DegN | 0.71 | 183822 |
| P1 | S | dHS = 0.44·DegN + 0.18·Bright1 - 0.84·Bright + 0.23·SolIrr | 0.52 | 1835069 |
| P2 | S | dHS = 0.42·Slope - 0.57·Bright | 0.63 | 522522 |

*Table 3. Mean, standard deviation (SD), Coefficient of Variation (CV) for snow depth (HS) and snow depth change (dHS) for different periods and areas. P1 was from 19 May 2015 to 01 June 2015 and P2 from 01 June 2015 to 24 June 2015. Values are given for only snow covered areas. Values for HS are given for the start date of the period. Values for dHS are given for the area which was snow covered at the end of the melt period.*

| Period | area | HS [m] | | | dHS [cm/d] | | |
|---|---|---|---|---|---|---|---|
| | | Mean | SD | CV | Mean | SD | CV |
| P1 | all | 1.26 | 1.16 | 0.92 | 6.22 | 1.22 | 0.20 |
| P2 | all | 1.33 | 1.13 | 0.85 | 7.57 | 1.19 | 0.16 |
| P1 | N | 1.28 | 0.93 | 0.73 | 6.86 | 1.22 | 0.18 |
| P2 | N | 0.98 | 0.73 | 0.74 | 6.76 | 1.35 | 0.20 |
| P1 | S | 1.25 | 1.27 | 1.01 | 5.72 | 0.97 | 0.17 |
| P2 | S | 1.54 | 1.27 | 0.83 | 7.86 | 0.98 | 0.12 |